

Structure Effects on Electro-Osmosis in Microporous Media

Moran Wang¹

School of Aerospace,
Tsinghua University,
Beijing 100084, China;
Earth and Environmental Sciences Division,
Los Alamos National Laboratory,
Los Alamos, NM 87545,
e-mail: moralwang@gmail.com;
mrwang@tsinghua.edu.cn

The structure effects on electro-osmosis in microporous media have been studied by modeling the multiphysical transport using our numerical framework. The three-dimensional microstructures of porous media are reproduced by a random generation-growth method, and then the nonlinear governing equations for the electrokinetic transport are solved by a highly efficient lattice Poisson–Boltzmann method. The simulation results indicate that the porous structure type (granular, fibrous, or network) influences the electro-osmotic permeability significantly. At the low porosity regime (<0.4), the network structure exhibits the highest electro-osmotic permeability because of its highest surface–volume ratio among the three types of structure at the same porosity. When the porosity is high (>0.5), the granular structure leads to the highest electro-osmotic permeability due to its lower shape resistance characteristics. The present modeling results improve our understanding of hydrodynamic and electrokinetic transport in geophysical systems, and help guide the design of porous electrodes in micro-energy systems. [DOI: 10.1115/1.4005711]

Keywords: electro-osmosis, porous media, multiphysical transport, lattice Boltzmann, environment and energy

1 Introduction

Electro-osmosis in porous media has been studied for nearly 200 years because of its importance in geophysical systems [1,2] since the electrokinetic effects were first observed by Reuss in 1809 [3]. In recent decades, there have been considerable and reawakening interests in the electro-osmosis in porous media because of the conspicuous applications in biomedical analysis [4–6], new techniques and designs for micro-energy (batteries and fuel cells) and power (pumps) systems [7–10], and geophysical system analysis [11,12]. Although there have been quite a few theoretical studies on electro-osmotic phenomena in porous media, it is still a big challenge to accurately and efficiently predict the multiphysical transport behaviors in porous media due to their complexities. There are three deficiencies in the existing theoretical models for predicting electro-osmosis in microporous media. First, most of the models are based on vanishingly thin electric double layers (EDL) [9,13] so that they are not suitable for dense micro and nanoscale porous media where the length scale of the small pores may be in the same order of the EDL thickness. Second, the theoretical models can hardly provide sufficient details in flow structure, which are necessary for deep understandings of the transport mechanism of electro-osmosis in porous media. Third, the real structures of porous media may have very different geometries and may fall into quite special range of porosity for various applications. Therefore, no general theoretical models have been reported to have a universal capability for performance prediction or mechanism analysis.

Owing to the rapid developments of computational techniques, various numerical methods have been developed in the past decade for modeling and predicting the electro-osmotic transport in porous media. Coelho et al. [14] developed a direct numerical solution for the electro-osmosis in porous media in the linear limit when the EDL thickness was much larger than the elementary grid size, and the method was applied to analyze the electro-osmotic phenomena in fractures [15] and compact clays [16,17]. Gupta et al. [18] recently extended their linear model to the

nonlinear region for high zeta potentials. Since the accuracy of their models depends strongly on the discretization step, their applications are limited by the computational costs. Only a few results with relatively coarse spatial discretization steps have been found to reach reasonable computation times [14,15,18–21]. Kang et al. [22] introduced the interval functions approximation [23] into the Poisson–Boltzmann equation to simplify the solution process and to improve the efficiency. Their method showed good performance to analyze electro-osmotic flows in packed microspheres [24,25]. Hlushkou et al. [26] proposed to combine a traditional finite-difference method for electrostatics with a lattice Boltzmann method for hydrodynamics, and investigated electro-osmosis in sphere arrays. Recently, Wang et al. [27,28] developed a lattice Poisson–Boltzmann method (LPBM) and employed it to analyze the electrokinetic transport in regular or random porous media [29–31]. However, most of these previous studies focused on granular microstructures of porous media. Actually, the natural solid structures of porous media vary significantly. A popular classification of porous structures is to distinguish them into three categories: granular, fibrous, and network structures. To our best knowledge, no contributions have reported on electro-osmotic transport in other than granular porous media, and therefore, the structure effects on the electro-osmotic permeability through different porous media with complex geometries.

The purpose of this work is to investigate the structure (granular, fibrous, or network) effects on electro-osmotic transport of electrolyte solutions through various porous media by our theoretical and numerical framework. The rest of this paper is arranged as follows. In Sec. 2, we introduce our mathematical framework, including a comprehensive algorithm for microstructure reproduction and a high-efficiency lattice evolution solver for a set of governing equations for the multiphysical transport processes. We present our simulation results and discussion in Sec. 3, where the structure effects on electro-osmotic transport in porous media are analyzed. Finally, we draw some conclusions from this study in Sec. 4.

2 Mathematical Framework

2.1 Structure Generation. Here we use the random generation-growth method to reproduce the random

¹Corresponding author.

Contributed by the Heat Transfer Division of ASME for publication in the JOURNAL OF HEAT TRANSFER. Manuscript received July 30, 2010; final manuscript received July 2, 2011; published online April 11, 2012. Assoc. Editor: Ping Cheng.

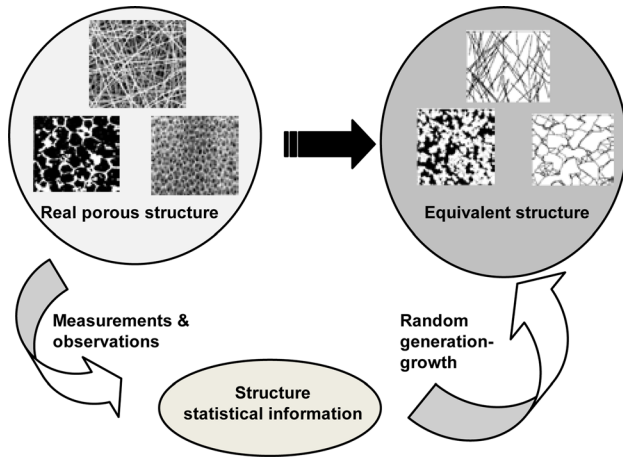


Fig. 1 Microstructure generation strategy

microstructure of multiphase materials [32]. The strategy of our method is illustrated in Fig. 1. We are not to photomap the actual porous structures but to generate the equivalent ones that reflect all the dominant factors of the structures necessary for the macroscopic properties. To achieve these, we first obtain the statistical information of the structures through measurements and then feed the information to the random generation-growth method for structure reproductions. The dominating statistical information of microstructures include shape and number density of particles, volume fractions of phases, morphology, anisotropy, and so on. Generally, the solid structures of porous media can be divided into three categories: granular, fibrous, and network structures. The generation methods for these three types are actually based on the same principle with corresponding differences in details.

For the granular solid structures, we first randomly locate the seeds of the solid particles in a grid system based on a distribution probability, s_d . Each cell will be assigned a random number by a uniform distribution function within (0, 1), whose random number is no greater than s_d will be chosen as a seed. Then, every element of the growing phase is expanded to its neighboring cells in all directions based on each given directional growth probability, D_i , where i represents the direction. Again for each growing element, new random numbers will be assigned to its neighboring cells. The neighboring cell in direction i will become part of the growing phase if its random number is no greater than D_i . Repeat the growing process until the volume fraction of the solid phase reaches its given value V_s [33].

For the fibrous solid structure, we randomly locate the fiber seeds based on a core distribution probability, s_d . For each fiber seed, we randomly assign an orientation angle θ within $[-\theta_{lim}, \theta_{lim}]$. Then we grow fibers from each core along both directions of the orientation θ for fiber length and crosswise for fiber thickness. We finalize the growth once fiber dimensions reach the specified values or the porosity attains the given level [34].

For the network structure, we again stochastically distribute the cores as the net nodes on a lattice system based on a given probability s_d , similar to the other generation processes. For each net node, we search outward to the neighboring nodes and randomly select N_n of them as the link nodes; here N is determined based on the features of specific porous media. Genetic algorithms or other searching algorithms could be used for this process. We then grow link lines from a net node to each of its N link nodes. The porosity is controlled by the density of seeds [35].

Comparing the real porous structures on the left-hand side in Fig. 1 and the generated equivalent structures on the right-hand side tells that the artificial structures show random natures as strong as the real ones. Meanwhile since the statistical information has been embedded within the generation process, the equivalent structures will reflect same macroscopic properties as the real

ones, which has been proved in static properties other than with flows [32].

2.2 Governing Equations. Consider a dilute electrolyte solution ($<1 \times 10^{-3}$ mol/l) flowing through a three-dimensional solid porous structure. Although the pore scale may be of tens of nanometers, the electrolyte can be treated as a continuum Newtonian fluid since the size is still much (ten-times) greater than the molecular diameters of a liquid solvent [36].

The mathematical models for electrokinetic transport are generally under the following conditions or assumptions: (i) the system is in chemical and dynamic equilibrium; (ii) the transport process is in steady state; (iii) the pore size is much larger than the liquid solvent molecular size; (iv) the ions in the Stern layer are rigidly attached to the surfaces and have no contribution to the bulk ionic current; (v) the flow is slow enough so that the ion convection effect is negligible; (vi) the bulk ionic concentration is not too high (<1 mol/l) or not too low (the Debye length is smaller than ten times the channel width) so that the Poisson–Boltzmann (PB) model is still applicable [36]; (vii) no other chemical reactions occur at surfaces except for chemical adsorption and dissociation. Under the conditions of negligible convection effect and moderate ionic concentration, the ion transport can be described by the weakly coupled Poisson–Boltzmann model instead of the highly coupled Poisson–Nernst–Planck model [37]. The governing equations for the electrokinetic transport for a monovalent electrolyte solution are as follows [37,38]:

$$\nabla^2 \psi = \frac{2en_\infty}{\epsilon_r \epsilon_0} \sinh\left(\frac{e\psi}{kT}\right) \quad (1)$$

$$\rho_e = -2en_\infty \sinh\left(\frac{e\psi}{kT}\right) \quad (2)$$

$$\nabla \cdot \mathbf{u} = 0, \quad (3)$$

$$\rho \mathbf{u} \cdot \nabla \mathbf{u} = -\nabla p + \mu \nabla^2 \mathbf{u} + \rho_e \mathbf{E}, \quad (4)$$

where ψ denotes the static electric potential, e the absolute value of proton charge, $\epsilon_r \epsilon_0$ the permittivity of the solution, n_∞ the bulk ionic concentration, k the Boltzmann's constant, T the temperature, \mathbf{u} the fluid velocity, ρ the fluid density, p the pressure, μ the viscosity, ρ_e the charge density, and \mathbf{E} the electric field strength.

The nonslip model is used for the hydrodynamic boundary condition on solid surfaces. Although the slip boundary conditions have been adopted in recent studies, a careful molecular study showed that the hydrodynamic boundary condition, slip or not, depends on the molecular interactions between fluid and solid and on the channel size [39–41]. For dilute solutions, the nonslip boundary condition was shown to be valid.

2.3 Lattice Poisson–Boltzmann Method. After the porous structure has been generated, the set of coupled hydrodynamic and electrodynamic governing equations for the electrokinetic flows subject to the appropriate boundary conditions are solved by our LPBM [27]. This method combines an electric potential evolution method on discrete lattices to solve the nonlinear Poisson equation (i.e., the lattice Poisson method) [42] with a density evolution method on the same set of discrete lattices to solve the Boltzmann–BGK equation (i.e., the lattice Boltzmann method) [27]. The equations are only solved in the liquid phase. More details about the lattice Poisson–Boltzmann (LPB) algorithm can be found in our previous work [28,30,31]. The three-dimensional 15-speed (D3Q15) scheme used in our previous work for three-dimensional electro-osmosis in porous media [31] was shown to be unstable at high zeta potentials and low porosities [43]. Therefore, we use a stable three-dimensional 19-speed (D3Q19) scheme to replace the D3Q15 scheme [43].

The discrete evolution equation to solve the fluid dynamics (Eqs. (3) and (4)) can be written as [44]

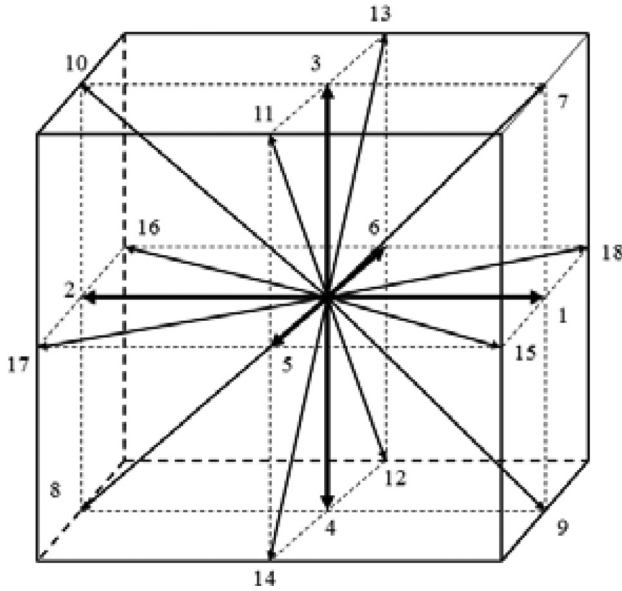


Fig. 2 The lattice direction system (α) for the three-dimensional 19-speed (D3Q19) model

$$f_{\alpha}(\mathbf{r} + \mathbf{e}_{\alpha}\delta_t, t + \delta_t) - f_{\alpha}(\mathbf{r}, t) = -\frac{1}{\tau_{\nu}} [f_{\alpha}(\mathbf{r}, t) - f_{\alpha}^{eq}(\mathbf{r}, t)] + \delta_t F_{\alpha} \quad (5)$$

where δ_t is the time step and \mathbf{e}_{α} denotes the discrete velocities for a D3Q19 system shown in Fig. 2

$$\mathbf{e}_{\alpha} = \begin{cases} (0, 0, 0) & \alpha = 0 \\ (\pm 1, 0, 0)c, (0, \pm 1, 0)c, (0, 0, \pm 1)c & \alpha = 1 \text{ to } 6 \\ (\pm 1, \pm 1, 0)c, (\pm 1, 0, \pm 1)c, (0, \pm 1, \pm 1)c & \alpha = 7 \text{ to } 18 \end{cases} \quad (6)$$

and τ_{ν} is the dimensionless relaxation time which is a function of the fluid viscosity, $\tau_{\nu} = 0.5 + 3\nu/\delta_x c$, with ν representing the kinetic viscosity, c the lattice speed, and δ_x the lattice constant (grid size). The lattice speed ($c = \delta_x/\delta_t$) is an adjustable parameter to reach an easy balance between accuracy and efficiency [45]. A large value of c ($c \gg 1$) yields a condition that approaches the limit of an incompressible fluid. An appropriate value of c should ensure τ_{ν} within (0.5, 2) [42].

For the D3Q19 model, the density equilibrium distribution f_{α}^{eq} takes the following form:

$$f_{\alpha}^{eq} = \omega_{\alpha} \rho \left[1 + 3 \frac{\mathbf{e}_{\alpha} \cdot \mathbf{u}}{c^2} + 9 \frac{(\mathbf{e}_{\alpha} \cdot \mathbf{u})^2}{2c^2} - \frac{3\mathbf{u}^2}{2c^2} \right] \quad (7)$$

with

$$\omega_{\alpha} = \begin{cases} 1/18 & \alpha = 0 \\ 1/18 & \alpha = 1 \text{ to } 6 \\ 1/36 & \alpha = 7 \text{ to } 18 \end{cases} \quad (8)$$

The external force in the discrete evolution equation is [46]

$$F_{\alpha} = \frac{3\rho_e \mathbf{E} \cdot (\mathbf{e}_{\alpha} - \mathbf{u})}{\rho c^2} f_{\alpha}^{eq} \quad (9)$$

The macroscopic density and velocity can be calculated by the same way in the D3Q15 scheme [31]. Similarly, the discrete evolution equation for electric potential distribution can be written as [27,42]

$$g_{\alpha}(\mathbf{r} + \Delta \mathbf{r}, t + \delta_{t,g}) - g_{\alpha}(\mathbf{r}, t) = -\frac{1}{\tau_g} [g_{\alpha}(\mathbf{r}, t) - g_{\alpha}^{eq}(\mathbf{r}, t)] + \left(1 - \frac{0.5}{\tau_g}\right) \delta_{t,g} \omega_{\alpha} g_s \quad (10)$$

where the equilibrium distribution of the electric potential evolution variable g in the D3Q19 scheme is

$$g_{\alpha}^{eq} = \begin{cases} 0 & \alpha = 0 \\ \psi/18 & \alpha = 1 \text{ to } 6 \\ \psi/18 & \alpha = 7 \text{ to } 18 \end{cases} \quad (11)$$

The time step for the electric potential evolution is $\delta_{t,g} = \delta_x/c_g$, where c_g is the lattice speed for the electric potential propagation [42]. The dimensionless relaxation time can be determined by a multiscale analysis of the discrete Boltzmann evolution equations. For the D3Q19 model [43,47], it is calculated by

$$\tau_g = \frac{9\chi}{5\delta_x c_g} + 0.5 \quad (12)$$

where χ is defined as potential diffusivity and set to unity in our simulations, c_g is also adjustable just to ensure the value of τ_g is within 0.5 and 2 [42,45]. After evolving on the discrete lattices, the macroscopic electric potential can be calculated using

$$\psi = \sum_{\alpha} (g_{\alpha} + 0.5\delta_{t,g} \omega_{\alpha}) \quad (13)$$

The evolution equation for electric potential distribution, Eq. (10), is valid for slow flows so that the electromagnetic susceptibility effect can be neglected. Although the lattice evolution method for the nonlinear Poisson equation is not as efficient as the multigrid solutions for simple geometries due to its long-wavelength limit, it is more suitable for geometrical complexity and parallel computing [43].

The hydrodynamic boundary conditions for the lattice Boltzmann method (LBM) have been studied extensively [28,48–52]. The conventional bounce-back rule is the most commonly used method; however, the nonslip boundary implemented by the conventional bounce-back rule is not exactly located at the boundary nodes, which will lead to inconsistencies when the LBM is coupled with other partial differential equation (PDE) solvers on the same grid set [30,49]. To overcome the inconsistencies between the LBM and other PDE solvers on the same grid set, one can replace the bounce-back rule with another “nonslip” boundary treatment, with the cost of losing easy implementation for complicated geometries. An alternative solution is to modify the boundary condition treatments of the PDE solver for the electric potential distribution to be consistent with the LBM with the conventional bounce-back rule. In this study, the nonequilibrium bounce-back rule [48] has been extended for both hydrodynamic and electrodynamic boundary treatments. Note that the bounce-back rule leads to a half-grid invasion of solid surface boundary into the liquid [30,50] so that the solid volume fraction needs to be recalculated. For the hydrodynamic boundaries, the following condition holds: $f_{\alpha}^{neq} = f_{\beta}^{neq}$, where the subscripts α and β represent the opposite directions. Analogously, the nonequilibrium “bounce-back” rule for the electric potential distribution at the wall surfaces is suggested as $g_{\alpha}^{neq} = -g_{\beta}^{neq}$. These boundary treatments are easy to implement for complicated geometries and have approximately second-order accuracy [48,49].

3 Results and Discussion

To study the structure effects on electro-osmosis in porous media, we first generate three-dimensional microstructures at different porosities for each type (granular, fibrous, or network), and then solve the governing equations for the multiphysical transport

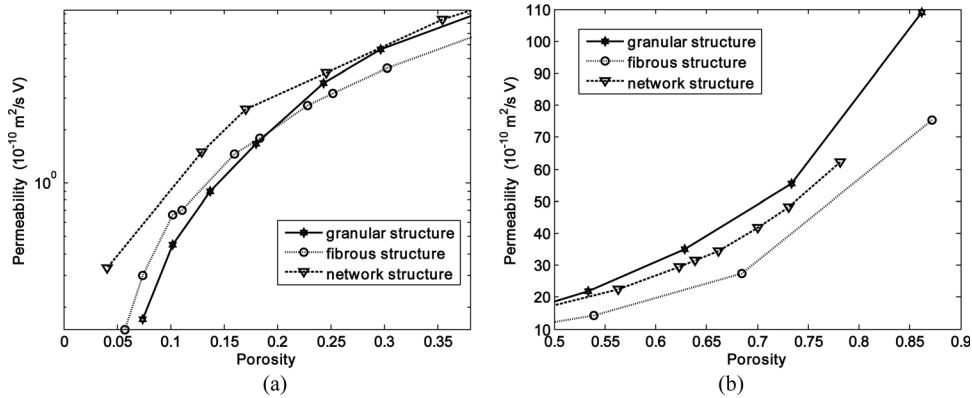


Fig. 3 The electro-osmotic permeability as functions of porosity at different porosity ranges (a) for the low porosity regime (0, 0.38) and (b) for the high porosity regime (0.5, 0.9)

by our high-efficiency lattice Poisson–Boltzmann method. After the velocity field is solved out, the electro-osmotic permeability is calculated by $\kappa_e = \bar{u}/E$ [53], where \bar{u} is the averaged velocity of electro-osmosis along the direction of the driving electrical field E .

In the following simulations, we focus on a micron cubic system which is divided into a $60 \times 60 \times 60$ uniform grid. Since stochastic factors have been introduced into the microstructure generation process, even simulations with the same parameters seldom produce exactly the same results. Like we did before, we run 3-5 trials for each case and use the averaged transport properties as the final result. For the current grid system, the fluctuation error is normally within 5% [31].

The fluid properties are the density $\rho = 10^3 \text{ kg/m}^3$, the dielectric constant $\epsilon_r \epsilon_0 = 6.95 \times 10^{-10} \text{ C}^2/\text{J m}$, and the dynamic viscosity $\mu = 0.889 \times 10^{-3} \text{ Pa s}$ [27]. The other modeling parameters are the temperature $T = 293 \text{ K}$, the surface zeta potential

$\zeta = -50 \text{ mV}$, the bulk ionic concentration $n_\infty = 1 \times 10^{-5} \text{ mol/l}$, and the external electrical field strength $E = 1 \times 10^6 \text{ V/m}$. For the cases considered in this work, the CPU time per simulation is less than 50 min for a relative error tolerance 10^{-6} every 100 time steps for both the electric potential and the flow velocity.

Figure 3 shows the electro-osmotic permeability as a function of porosity of porous microstructures for the three types of structures. We distinguish the porosity into two regimes because of not only their quite different features but also their audience of best interests. In the low porosity regime from 0 to 0.38 as shown in Fig. 3(a), which is of interest in many geophysical applications, the electro-osmotic permeability varies significantly with the porosity, nearly two orders of magnitude over this very narrow porosity range. In this porosity regime, the network structure shows the highest electro-osmotic permeability. The granular structure with a porosity lower than 0.15 or the fibrous structure with that higher than 0.2 leads to the lowest electro-osmotic

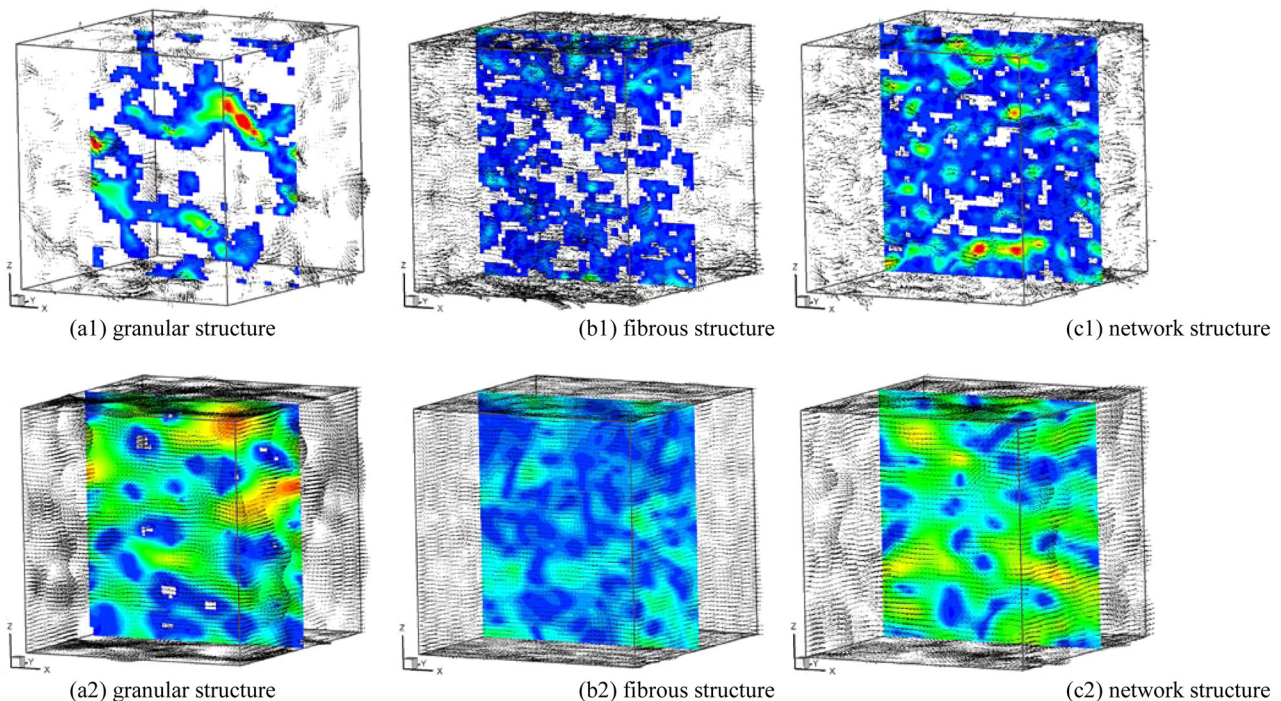


Fig. 4 Velocity fields for three types of structures for different porosities. The porosity of structures for a1, b1, and c1 is 0.1 and that for a2, b2, and c2 equals 0.73. The vectors denote the three-dimensional velocity field. The contours shows the values of velocity in x-direction at mid-plane ($y = 0.5$). The scales for vector and contour are same for the three structures, respectively. For the contour maps, the solid parts are blocked for clear show.

permeability. Especially when the porosity is quite low, for example, lower than 0.1, the structure effect on permeability is enhanced by a lower porosity. At the porosity around 0.1, the electro-osmotic permeability for the fibrous structure is nearly 50% higher than that for the granular structure, but 50% lower than that for the network structure. In the other porosity regime from 0.5 to 0.9, which may be of interest in energy or power systems, the granular structure exhibits a consistent advantage in electro-osmotic permeability over the other two types of structures. The fibrous structure leads to the lowest electro-osmotic permeability in the entire high porosity regime, which is nearly half of that for granular structures at the same porosity. The results in Fig. 3 will help to design or optimize microstructures when electro-osmosis in porous media is applied in environmental and energy systems.

The reason why the structure effects on electro-osmotic permeability in porous media exhibit so different characteristics in low and high porosity regimes could be explained from the details of flow structures. Figure 4 shows the flow fields for the three types of structures at a low porosity 0.1 (a1, b1, c1) and a high porosity 0.73 (a2, b2, c2). The vectors denote the three-dimensional velocity field. The contours show the values of velocity in x -direction at mid-plane ($y=0.5$). The scales for vector and contour are same for the three structures, respectively. For the contour maps, the solid parts are blocked for clear show. The results indicate that the structure effect on electro-osmotic permeability is actually a comprehensive result from two competing factors: the surface–volume ratio whose higher value will enhance the permeability and the shape resistance which weakens the flow velocity. For the low porosity regime, as shown in Fig. 4 (a1, b1, c1), the surface–volume ratio differs significantly between the three types of structures, which affects the electro-osmotic driving force. The network structure has the highest surface–volume ratio while the granular owns the lowest one. As a result, the network structure exhibits the highest electro-osmotic permeability and the granular the lowest when the porosity is very low, just as shown in Fig. 3(a). When the porosity is high (>0.5), the electric double layer will be fully developed despite the structure types and the shape resistance to the flow will play a more important role. The granular structure owns the lowest shape resistance and leads to the highest electro-osmotic permeability as the result.

4 Conclusions

We present a numerical framework in this contribution for the multiphysical transport in electro-osmosis through microporous media with granular random structures. The framework includes random generation-growth method to reproduce the three-dimensional microstructures of porous media and a high-efficiency lattice Poisson–Boltzmann algorithm to solve the nonlinear governing equations for the electrokinetic transport. The structure effects on electro-osmosis in porous media have been, therefore, studied by modeling the multiphysical transport using our numerical framework. The simulation results indicate that the porous structure type (granular, fibrous, or network) influences the electro-osmotic permeability significantly. At the low porosity regime (<0.4), the network structure exhibits the highest electro-osmotic permeability because of its highest surface–volume ratio among the three types of structure. When the porosity is high (>0.5) the granular structure leads to the highest electro-osmotic permeability due to its lower shape resistance characteristics. The present modeling results may improve our understanding of hydrodynamic and electrokinetic transport in geophysical systems, and help guide the design of porous electrodes in micro-energy systems.

Acknowledgment

The author would like to thank helpful discussions with Professor S. Chen, Dr. Q.J. Kang, Dr. B.A. Robinson, and Professor

N. Pan. This work is currently supported by NSFC (No. 51176089) and the startup grants from Tsinghua University and was previously supported by the J. R. Oppenheimer Fellowship from Los Alamos National Laboratory.

References

- [1] Alexander, A. E., and Jonson, P., 1949, *Colloid Science*, Clarendon, Oxford.
- [2] Tikhomolova, K. P., 1993, *Electro-Osmosis*, Ellis Horwood, New York.
- [3] Reuss, F., 1809, "Sur Un Nouvel Effect De L'electricite Galvanique," *Memoires de la Societe Imperiale de Naturalistes de Moscou*, **2**, pp. 327–337.
- [4] Banga, A. K., 1998, *Electrically Assisted Transdermal and Topical Drug Delivery*, Taylor & Francis, London.
- [5] Masliyah, J. H., and Bhattacharjee, S., 2006, *Electrokinetic and Colloid Transport Phenomena*, Wiley, New York.
- [6] Oosterbroek, R. E., and Berg, A. V. D., 2003, *Lob-on-a-Chip: Miniaturized Systems for (Bio) Chemical Analysis and Sintesis*, Elsevier, Boston.
- [7] Ren, Y. Q., and Stein, D., 2008, "Slip-Enhanced Electrokinetic Energy Conversion in Nanofluidic Channels," *Nanotechnology*, **19**(19), pp. 195707.
- [8] Yao, S. H., and Santiago, J. G., 2003, "Porous Glass Electroosmotic Pumps: Theory," *J. Colloid Interface Sci.*, **268**(1), pp. 133–142.
- [9] Zeng, S. L., Chen, C. H., Mikkelsen, J. C., and Santiago, J. G., 2001, "Fabrication and Characterization of Electroosmotic Micropumps," *Sens. Actuat. B Chem.*, **79**(2–3), pp. 107–114.
- [10] Jianhu, N., Yitong, C., Boehm, R. F., and Katukota, S., 2008, "A Photoelectrochemical Model of Proton Exchange Water Electrolysis for Hydrogen Production," *J. Heat Transf.*, **130**(4), p. 042409.
- [11] Depaolo, D. J., and Orr, Jr. F. M., 2007, "Basic Research Needs for Geosciences: Facilitating 21st Century Energy Systems," Technical Report No. Office of basic energy sciences, U.S. Department of Energy, Report No. 935430.
- [12] Kitamura, A., Fujiwara, K., Yamamoto, T., Nishikawa, S., and Moriyama, H., 1999, "Analysis of Adsorption Behavior of Cations Onto Quartz Surface by Electrical Double-Layer Model," *J. Nucl. Sci. Technol.*, **36**(12), pp. 1167–1175.
- [13] Laser, D. J., and Santiago, J. G., 2004, "A Review of Micropumps," *J. Micro-mech. Microeng.*, **14**(6), pp. R35–R64.
- [14] Coelho, D., Shapiro, M., Thovert, J. F., and Adler, P. M., 1996, "Electroosmotic Phenomena in Porous Media," *J. Colloid Interface Sci.*, **181**(1), pp. 169–190.
- [15] Marino, S., Coelho, D., Bekri, S., and Adler, P. M., 2000, "Electroosmotic Phenomena in Fractures," *J. Colloid Interface Sci.*, **223**(2), pp. 292–304.
- [16] Rosanne, M., Paszkuta, M., Thovert, J. F., and Adler, P. M., 2004, "Electro-Osmotic Coupling in Compact Clays," *Geophys. Res. Lett.*, **31**(18), p. 020770.
- [17] Rosanne, M., Paszkuta, M., and Adler, P. M., 2006, "Electrokinetic Phenomena in Saturated Compact Clays," *J. Colloid Interface Sci.*, **297**(1), pp. 353–364.
- [18] Gupta, A. K., Coelho, D., and Adler, P. M., 2006, "Electroosmosis in Porous Solids for High Zeta Potentials," *J. Colloid Interface Sci.*, **303**(2), pp. 593–603.
- [19] Levine, S., Marriott, J. R., Neale, G., and Epstein, N., 1975, "Theory of Electrokinetic Flow in Fine Cylindrical Capillaries at High Zeta Potentials," *J. Colloid Interface Sci.*, **52**(1), pp. 136–149.
- [20] Chien-Hsin, C., 2009, "Thermal Transport Characteristics of Mixed Pressure and Electro-Osmotically Driven Flow in Micro- and Nanochannels With Joule Heating," *J. Heat Transf.*, **131**(2), p. 022401.
- [21] Bhattacharyya, S., and Nayak, A. K., "Combined Effect of Surface Roughness and Heterogeneity of Wall Potential on Electroosmosis in Microfluidic/Nanofluidic Channels," *J. Fluid Eng.*, p. 041103.
- [22] Kang, Y. J., Yang, C., and Huang, X. Y., 2002, "Electroosmotic Flow in a Capillary Annulus With High Zeta Potentials," *J. Colloid Interface Sci.*, **253**(2), pp. 285–294.
- [23] Philip, J. R., and Wooding, R. A., 1970, "Solution of Poisson-Boltzmann Equation About a Cylindrical Particle," *J. Chem. Phys.*, **52**(2), pp. 953–959.
- [24] Kang, Y. J., Yang, C., and Huang, X. Y., 2004, "Analysis of the Electroosmotic Flow in a Microchannel Packed with Homogeneous Microspheres Under Electrokinetic Wall Effect," *Int. J. Eng. Sci.*, **42**(19–20), pp. 2011–2027.
- [25] Kang, Y. J., Yang, C., and Huang, X. Y., 2005, "Analysis of Electroosmotic Flow in a Microchannel Packed With Microspheres," *Microfluid. Nanofluid.*, **1**(2), pp. 168–176.
- [26] Hlushkou, D., Seidel-Morgenstern, A., and Tallarek, U., 2005, "Numerical Analysis of Electroosmotic Flow in Dense Regular and Random Arrays of Impermeable, Nonconducting Spheres," *Langmuir*, **21**(13), pp. 6097–6112.
- [27] Wang, J. K., Wang, M., and Li, Z. X., 2006, "Lattice Poisson-Boltzmann Simulations of Electro-Osmotic Flows in Microchannels," *J. Colloid Interface Sci.*, **296**(2), pp. 729–736.
- [28] Wang, M. R., Wang, J. K., and Chen, S. Y., 2007, "Roughness and Cavitations Effects on Electro-Osmotic Flows in Rough Microchannels Using the Lattice Poisson-Boltzmann Methods," *J. Comput. Phys.*, **226**(1), pp. 836–851.
- [29] Wang, M., Wang, J. K., Chen, S. Y., and Pan, N., 2006, "Electrokinetic Pumping Effects of Charged Porous Media in Microchannels Using the Lattice Poisson-Boltzmann Method," *J. Colloid Interface Sci.*, **304**(1), pp. 246–253.
- [30] Wang, M., Pan, N., Wang, J. K., and Chen, S. Y., 2007, "Lattice Poisson-Boltzmann Simulations of Electroosmotic Flows in Charged Anisotropic Porous Media," *Commun. Comput. Phys.*, **2**, pp. 1055–1070.
- [31] Wang, M., and Chen, S., 2007, "Electroosmosis in Homogeneously Charged Micro- and Nanoscale Random Porous Media," *J. Colloid Interface Sci.*, **314**(1), pp. 264–273.

- [32] Wang, M., and Pan, N., 2008, "Predictions of Effective Physical Properties of Complex Multiphase Materials," *Mater. Sci. Eng.: R*, **63**(1), pp. 1–30.
- [33] Wang, M. R., Wang, J. K., Pan, N., and Chen, S. Y., 2007, "Mesoscopic Predictions of the Effective Thermal Conductivity for Microscale Random Porous Media," *Phys. Rev. E*, **75**(3), p. 036702.
- [34] Wang, M. R., He, J. H., Yu, J. Y., and Pan, N., 2007, "Lattice Boltzmann Modeling of the Effective Thermal Conductivity for Fibrous Materials," *Int. J. Therm. Sci.*, **46**(9), pp. 848–855.
- [35] Wang, M., and Pan, N., 2008, "Modeling and Prediction of the Effective Thermal Conductivity of Random Open-Cell Porous Foams," *Int. J. Heat Mass Transf.*, **51**(5–6), pp. 1325–1331.
- [36] Wang, M., and Chen, S. Y., 2008, "On Applicability of Poisson-Boltzmann Equation for Micro- and Nanoscale Electroosmotic Flows," *Commun. Comput. Phys.*, **3**(5), pp. 1087–1099.
- [37] Li, D. Q., 2004, *Electrokinetics in Microfluidics*, Academic Press, Oxford.
- [38] Schoch, R. B., Han, J. Y., and Renaud, P., 2008, "Transport Phenomena in Nanofluidics," *Rev. Mod. Phys.*, **80**(3), pp. 839–883.
- [39] Joly, L., Ybert, C., Trizac, E., and Bocquet, L., 2004, "Hydrodynamics Within the Electric Double Layer on Slipping Surfaces," *Phys. Rev. Lett.*, **93**(25), p. 257805.
- [40] Dufreche, J. F., Marry, V., Maliková, N., and Turq, P., 2005, "Molecular Hydrodynamics for Electro-Osmosis in Clays: From Kubo to Smoluchowski," *J. Mol. Liquids*, **118**(1–3), pp. 145–153.
- [41] Wang, M., Liu, J., and Chen, S., 2007, "Similarity of Electroosmotic Flows in Nanochannels," *Mol. Sim.*, **33**(3), pp. 239–244.
- [42] Wang, J. K., Wang, M., and Li, Z. X., 2008, "Lattice Evolution Solution for the Nonlinear Poisson-Boltzmann Equation in Confined Domains," *Commun. Nonlinear Sci. Numer. Simul.*, **13**(3), pp. 575–583.
- [43] Wang, M., and Kang, Q. J., 2009, "Electrokinetic Transport in Microchannels With Random Roughness," *Analyt. Chem.*, **81**(8), pp. 2953–2961.
- [44] Chen, S., and Doolen, G. D., 1998, "Lattice Boltzmann Method for Fluid Flows," *Annu. Rev. Fluid Mech.*, **30**, pp. 329–364.
- [45] Wang, J. K., Wang, M., and Li, Z. X., 2007, "A Lattice Boltzmann Algorithm for Fluid-Solid Conjugate Heat Transfer," *Int. J. Therm. Sci.*, **46**(3), pp. 228–234.
- [46] He, X., Chen, S., and Doolen, G. D., 1998, "A Novel Thermal Model for the Lattice Boltzmann Method in Incompressible Limit," *J. Comput. Phys.*, **146**(1), pp. 282–300.
- [47] Peng, Y., Shu, C., and Chew, Y. T., 2004, "A 3d Incompressible Thermal Lattice Boltzmann Model and Its Application to Simulate Natural Convection in a Cubic Cavity," *J. Comput. Phys.*, **193**(1), pp. 260–274.
- [48] Zou, Q., and He, X., 1997, "On Pressure and Velocity Boundary Conditions for the Lattice Boltzmann Bgk Model," *Phys. Fluids*, **9**(6), pp. 1591–1598.
- [49] Rohde, M., Kandhai, D., Derksen, J. J., and Van Den Akker, H. E. A., 2003, "Improved Bounce-Back Methods for No-Slip Walls in Lattice-Boltzmann Schemes: Theory and Simulations," *Phys. Rev. E*, **67**(6), p. 066703.
- [50] Chen, S. Y., Martinez, D., and Mei, R. W., 1996, "On Boundary Conditions in Lattice Boltzmann Methods," *Phys. Fluids*, **8**(9), pp. 2527–2536.
- [51] Noble, D. R., Chen, S. Y., Georgiadis, J. G., and Buckius, R. O., 1995, "A Consistent Hydrodynamic Boundary Condition for the Lattice Boltzmann Method," *Phys. Fluids*, **7**(1), pp. 203–209.
- [52] D'orazio, A., and Succi, S., 2004, "Simulating Two-Dimensional Thermal Channel Flows by Means of a Lattice Boltzmann Method With New Boundary Conditions," *Future Gen. Comput. Syst.*, **20**(6), pp. 935–944.
- [53] Rastogi, R. P., and Jha, K. M., 1966, "Cross-Phenomenological Coefficients. 3. Studies on Electroosmosis," *J. Phys. Chem.*, **70**(4), pp. 1017–1024.